JOURNAL OF APPLIED ELECTROCHEMISTRY 16 (1986) 851–866

*Selectivity analysis in electrochemical reactors. II. Engineering models of a batch reactor with a complex reaction sequence**

L. WEISE, G. VALENTIN, A. STORCK

Laboratoire des Sciences du Génie Chimique, CNRS–ENSIC, 1 rue Grandville, 54042 Nancy Cedex, France

Received 11 March 1986; revised 14 July 1986

This paper presents a mathematical model of a batch stirred-tank electrochemical reactor where a required cathodic reduction reaction is coupled with a complex reaction sequence between the reactant and the key product. The set of coupled, non-linear differential equations is solved numerically and simple dimensionless quantities characterizing the cell performance and selectivity are derived. The experimental results presented in Part I of this paper are found to be in excellent agreement with the model. In the particular case where the homogeneous chemical reactions may be neglected in the cathodic diffusion boundary layer, a simplified analytical expression of the process selectivity is proposed. This quantifies the effects of the operating conditions by means of a single dimensionless criterion.

Nomenclature

A_e	electrode area
a_e	specific electrode area
C_A, C_B, C_C	molar concentrations of species A, B, C
C_{AS}, C_{BS}, C_{CS}	bulk molar concentrations
C_{AO}	initial concentration of species A
C_A^+, C_B^+	reduced concentrations (with respect to C_{AS} – section 2)
C_{AO}^+, C_{BO}^+	reduced concentrations (with respect to C_{AO})
C_{BS}^*	$= C_{BS}/C_{AS}$
$C_{AS,i}^+$; $C_{BS,i}^+$	bulk concentrations in the ith reactor normalized with respect to C_{AO}
D_A, D_B	molecular diffusion coefficients
D_B^+	$= D_B/D_A$
E	electrode potential
F	Faraday's constant
Ha_0, Ha	Hatta numbers defined with respect to C_{AO} or C_{AS}
i	current density
i_L	limiting current density
i^*	dimensionless current density (Equation 6)
k_{ci}	chemical rate constants involved in scheme I
k_c	chemical rate constant of scheme II
k_d	mass transfer coefficient
K_1, K_2	dimensionless parameters defined in Equation 13
K	dimensionless parameter defined in Equation 17
N	impeller rotation speed
Q_v	volumetric flowrate
r_i	chemical reaction rate
R_A	conversion factor of species A
S	product selectivity
T	temperature
t	time
t^+	dimensionless time $= t(k_d a_e)$
V	volume of catholyte
X_A, X_B, X_C	molar fractions, i.e. C_{AS}/C_{AO}; C_{BS}/C_{AO}; C_{CS}/C_{AO}
y	coordinate perpendicular to the electrode

* This paper was presented at the meeting on 'Electroorganic Process Engineering' held in Perpignan, France, 19–20 September 1985.

0021-891X/86 $03.00 + .12

y^+	reduced coordinate $= y/\delta$	*Subscripts*	
ν_e	number of electrons involved in the reduction	f	final
		L	limiting
τ	space time	0	initial (time = 0)
		S	in the bulk of the electrolyte

1. Introduction

The first part of this study [1] presented an experimental investigation of the effect of important hydrodynamic, electrochemical and geometric parameters on the performance of a batch stirred-tank reactor, with a specific example of an electrochemical reduction for a required product coupled with homogeneous chemical side reactions. It was shown that different operating conditions of the cell may considerably modify the time distribution of the reaction rate and the concentrations of the electroactive species for a potentiostatic operation and, consequently, play a significant role in the overall process selectivity.

The numerous interconnections between different physical, chemical and electrochemical phenomena mean that the choice of the best operating conditions and cell design requires a general theoretical analysis of this problem based on a chemical engineering approach. Part I presented the overall reaction scheme for the electroreduction of *N*-nitroso-2-methylindoline to *N*-amino-2-methylindoline coupled with unwanted homogeneous reaction. Here in Part II we present a theoretical study of some aspects of the coupling between electrochemical and chemical reactions and, in particular:

(i) the effect of the chemical rate constants on the operating current density under potentiostatic conditions.

(ii) the modelling of a batch stirred-tank electrochemical reactor based on the film model.

The set of coupled differential equations is solved numerically and the comparison between the calculations and the experimental results is presented.

An analytical solution is derived for the overall selectivity which depends on a single dimensionless parameter in the case where the chemical rate constant is sufficiently low for the chemical reaction in the boundary layer at the working electrode to be neglected.

The incorporation of complex reaction sequences in engineering models of electrolytic cells was the subject of a recent paper [2], which dealt with the paired synthesis of propylene oxide in an undivided cell as a convenient system for model studies. This paper gave an excellent review of the mathematical tools for simulating cell and process behaviour.

The present paper presents a similar approach for the particular case of the synthesis *N*-amino-2-methylindoline with the additional objectives of deriving simple dimensionless quantities characterizing the process selectivity and of comparing the model to the experimental results.

2. Theoretical formulation: effect of the chemical rate constants on the operating current density (potentiostatic operation and static analysis)

2.1. *Basis of the model*

Let us consider the mechanism

$$A + \nu_e\, e \longrightarrow B$$

$$A + B \longrightarrow 2C$$

where the homogeneous chemical reaction is characterized by the rate constant, k_c, in its simplified form (scheme II of Part I). For a batch stirred-tank reactor, we define two zones inside the cell (see Fig. 1):

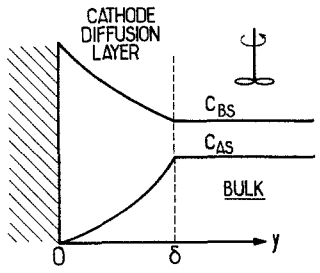

Fig. 1. Schematic diagram of the two zones defined in the cell.

(i) the bulk where there is no spatial concentration gradient

(ii) the film near the working electrode (cathode), where the gradients are located.

At a given instant the concentrations of the reacting species in the bulk are C_{AS} and C_{BS}.

The mass balances of A and B inside the diffusion layer are as follows

$$\begin{cases} D_A \dfrac{d^2C_A}{dy^2} - k_c C_A C_B = 0 & (1) \\ D_B \dfrac{d^2C_B}{dy^2} - k_c C_A C_B = 0 & (2) \end{cases}$$

Under potentiostatic limiting current conditions, the following boundary conditions apply for Equations 1 and 2

$$y = \delta;\ C_A = C_{AS};\ C_B = C_{BS};$$

$$y = 0 \begin{cases} C_A = 0 \\ D_A \left(\dfrac{dC_A}{dy}\right) = -D_B \left(\dfrac{dC_B}{dy}\right) = \dfrac{i}{v_e F} \end{cases}$$

The definition of a dimensionless quantity relating the competition between the chemical and electrochemical reaction rates is derived using the following reduced variables:

$$y^+ = y/\delta \qquad (3_1)$$

$$C_A^+ = C_A/C_{AS} \qquad (3_2)$$

$$C_B^+ = C_B/C_{AS} \qquad (3_3)$$

$$D_B^+ = D_B/D_A \qquad (3_4)$$

$$Ha^2 = \frac{k_c \delta^2 C_{AS}}{D_A} \qquad (3_5)$$

Equations 1 and 2 are then reduced to

$$\frac{d^2C_A^+}{dy^{+2}} - Ha^2 C_A^+ C_B^+ = 0 \qquad (4)$$

$$D_B^+ \frac{d^2C_B^+}{dy^{+2}} - Ha^2 C_A^+ C_B^+ = 0 \qquad (5)$$

with the boundary conditions:

$$y^+ = 1;\ C_A^+ = 1;\ C_B^+ = \frac{C_{BS}}{C_{AS}} = C_{BS}^*$$

$$y^+ = 0 \begin{cases} C_A^+ = 0 \\ \dfrac{dC_A^+}{dy^+} = -D_B^+ \dfrac{dC_B^+}{dy^+} = \dfrac{i}{v_e F k_d C_{AS}} = i^* \end{cases} \qquad (6)$$

with

$$k_d = D_A/\delta$$

The dimensionless number, Ha, defined by Equation 3_5 is the Hatta number. This number plays an important role in transfer phenomena with chemical reaction, and its significance has been outlined in literature dealing with multiphase reactors [3, 4]. Ha^2 may be also written in the following form:

$$Ha^2 = \frac{k_c \delta^2 C_{AS}}{D_A} = \frac{k_c C_{AS}^2 (\delta A_e)}{k_d A_e C_{As}} \tag{7}$$

The numerator of Equation 7 gives the instantaneous maximum flux of A by chemical reaction in the diffusion layer, whereas the denominator is the limiting diffusional flux if no chemical reaction takes place. Therefore Ha^2 gives a quantitative evaluation of the competition between the chemical and electrochemical reaction rates.

In Equation 6, i^* denotes a dimensionless form of the current density which gives the ratio of i to the limiting current density, i_L, corresponding to the concentration C_{AS} with no chemical reaction ($i_L = v_e F k_d C_{AS}$). Therefore i^*, which is between 0 and 1, measures the limitation of the current density by the chemical reaction inside the diffusion layer.

2.2. *The solution technique*

In the general case, and for a given value of C_{BS}^*, no analytical solution of Equations 4 and 5 exists and numerical integration is required. This integration can be greatly simplified by using the fact that

$$\frac{d^2 C_A^+}{dy^{+2}} = D_B^+ \frac{d^2 C_B^+}{dy^{+2}} \tag{8}$$

Two successive integrations of Equation 8 lead to the following relation between C_A^+ and C_B^+:

$$C_A^+ - 1 = D_B^+ (C_B^+ - C_{BS}^*) + 2(y^+ - 1) i^* \tag{9}$$

Equation 4 is then solved, taking into account Equation 9 which relates C_B^+ to C_A^+. For given values of Ha^2 and C_{BS}^*, the differential equation has been solved numerically through a five-order Runge–Kutta method from $y^+ = 0$ to $y^+ = 1$. The boundary condition at $y^+ = 0$ ($i^* = dC_A^+/dy^+$) has been estimated by a numerical optimization method (Simplex; [5]), which minimizes the error of the boundary conditions at $y^+ = 1$ ($C_A^+ = 1$ and $C_B^+ = C_{BS}^*$).

2.3. *Discussion of the model predictions*

For $D_B^+ = 0.62$ which corresponds to the experimental results of Part I and different values of C_{BS}^*, Fig. 2 presents the calculated variations of the dimensionless current density, i^*, with the Hatta number; Fig. 3a–c report some theoretical concentration profiles of A and B inside the diffusion boundary layer.

Examination of these figures leads to the following conclusions.

(i) For sufficiently small values of the Hatta number, i^* remains close to 1 and $i = i_L = v_e F k_d C_{AS}$. In this case i is limited by the electrochemical reaction and the concentration profiles are linear (see Fig. 3). The transition point from which i^* begins to decrease below 1 depends on the value of C_{BS}^* and is obtained for smaller Ha values when C_{BS}^* increases.

(ii) For higher values of Ha (i.e. higher chemical rate constants, k_c, and/or bulk concentrations, C_{AS}), i becomes limited by the homogeneous chemical reaction and i^* decreases. The limit of i^* depends on C_{BS}^* (ratio of C_{BS} to C_{AS}); an interesting result is that the value of this limit can be different from zero for small bulk concentrations of B. As an example, the limit is 0.5 for $C_{BS}^* = 0$ (see

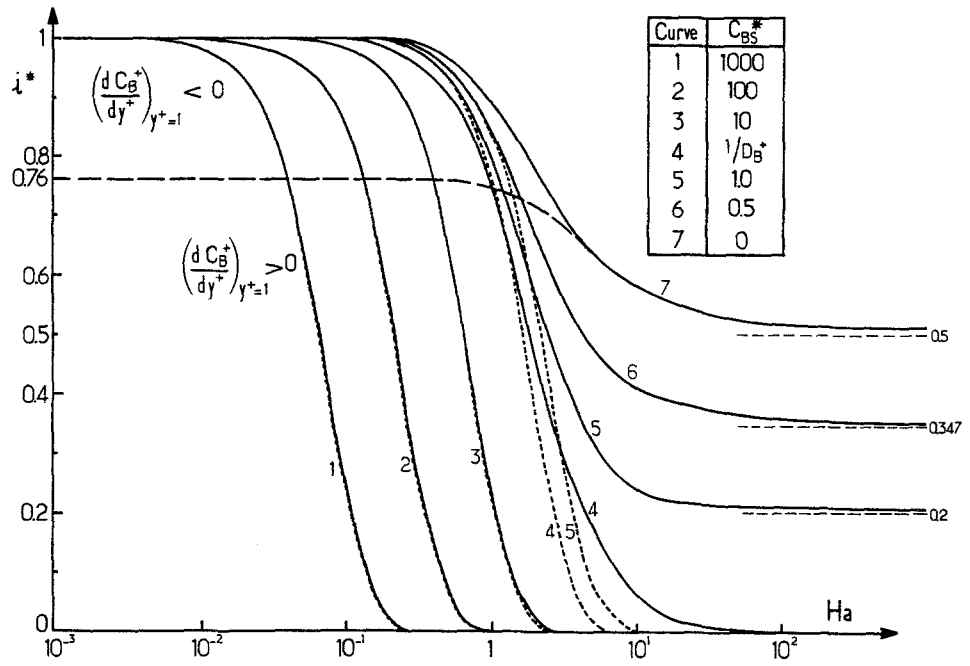

Fig. 2. Calculated variations of the normalized current density, i^*, with the Hatta number ($D_B^+ = 0.62$). Dashed curves = Equation 11.

Fig. 2). Indeed, Equation 9 written for $y^+ = 0$ where $C_A^+ = 0$ leads to the following expression:

$$i^* = \frac{1 + D_B^+ [(C_B^+)_{y^+=0} - C_{BS}^*]}{2}$$

and consequently (due to the fact that $(C_B^+)_{y^+=0} > 0$):

$$i^* > \frac{1 - D_B^+ C_{BS}^*}{2} \tag{10}$$

for $C_{BS}^* = 0$; $i^* > 0.5$.

It follows from this that:

(i) for $C_{BS}^* < 1/D_B^+$, the limit of i^* has a finite value different from zero, but smaller than 0.5

(ii) for $C_{BS}^* > 1/D_B^+$, the limit of i^* is zero when $Ha \to \infty$.

This result also appears clearly in Fig. 3 by considering the final slope (for $Ha \to \infty$) $[dC_A^*/ dy^+]_{y^+=0} = i^*$ of the concentration profiles of species A.

Obtaining a finite value of i^* when $Ha \to \infty$ means that the current density would not drop to zero even with an instantaneous chemical reaction between A and B. In such conditions (where $C_{BS}^* < 1/D_B^+$), B is the limiting reactant in the reaction A + B $\xrightarrow{(C)}$ 2C; this point explains the observed phenomenon. Finally it should be mentioned that there is a possibility of obtaining profiles of B with a minimum inside the boundary layer (see, for example, Fig. 3b, c).

In the i^* versus Ha plot of Fig. 2 the dashed line, which starts from $i^* = 0.76$, defines two zones. In the upper part, C_B^+ decreases in the layer from the electrode to the bulk, whereas in the lower part a minimum value is obtained.

2.4. *A simplified model*

As mentioned previously no analytical solution of Equations 4 and 5 exists in the general case, but

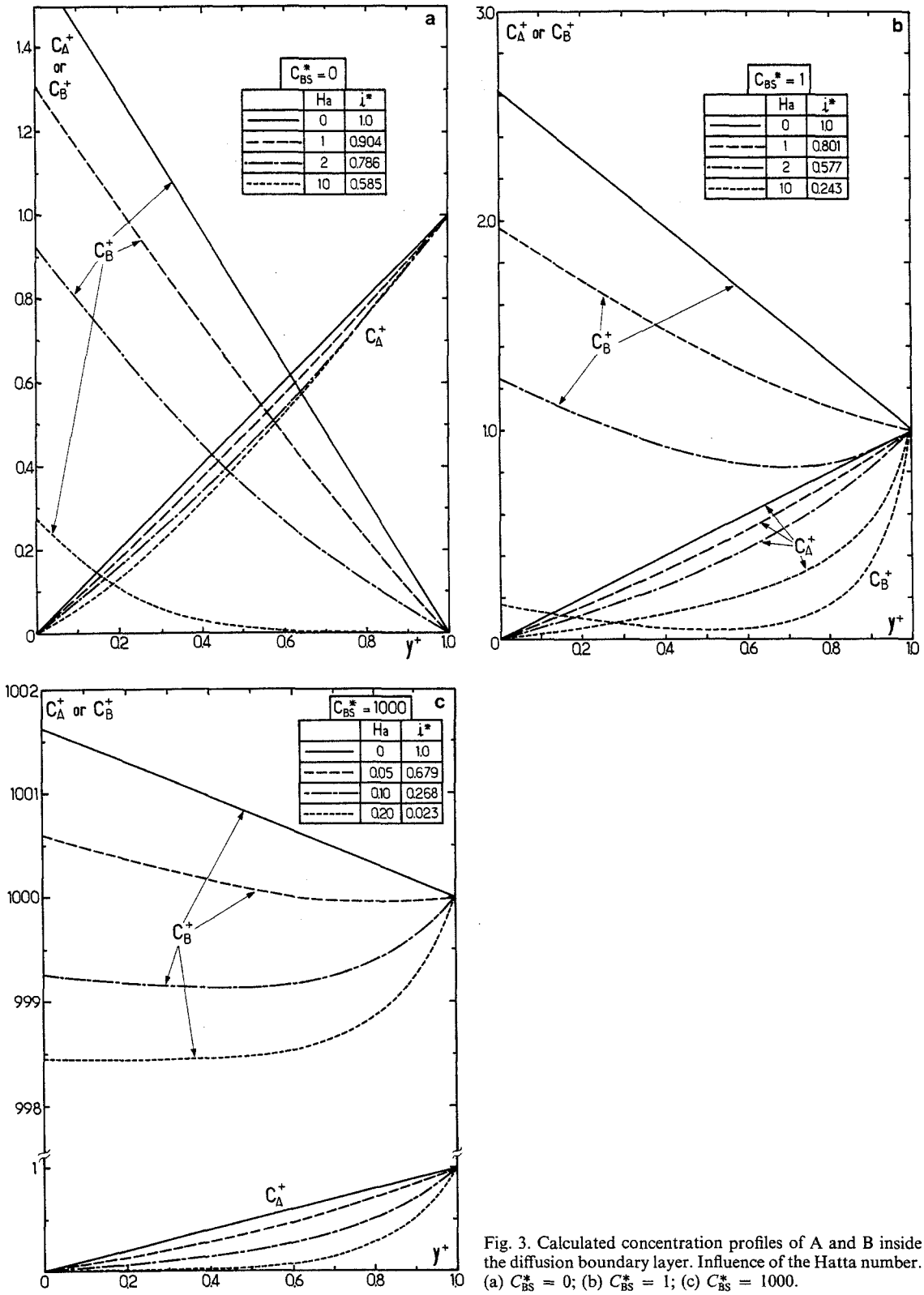

Fig. 3. Calculated concentration profiles of A and B inside the diffusion boundary layer. Influence of the Hatta number. (a) $C_{BS}^* = 0$; (b) $C_{BS}^* = 1$; (c) $C_{BS}^* = 1000$.

for large values of C_{BS}^* the integration may be performed by assuming, as a first approximation, that C_B^+ = constant = C_{BS}^* in the boundary layer. In this case one easily obtains the following analytical expressions for C_A^+ and i^*:

$$C_A^+ = \frac{sh\,[Ha(C_{BS}^*)^{\frac{1}{2}}y^+]}{sh\,[Ha(C_{BS}^*)^{\frac{1}{2}}]}$$

and

$$i^* = \left(\frac{dC_A^+}{dy^+}\right)_{y^+=0} = \frac{Ha\,(C_{BS}^*)^{\frac{1}{2}}}{sh\,[Ha(C_{BS}^*)^{\frac{1}{2}}]} \tag{11}$$

The comparison of the values of i^* given by Equation 11 and those calculated by numerical integration is shown in Fig. 2, which indicates that Equation 11 holds for $C_{BS}^* > 10$. The main conclusion of this section, concerning a steady state analysis at a given instant inside a batch reactor, is that i in its dimensionless form, i^*, only depends on two dimensionless quantities, i.e. the Hatta number and C_{BS}^*, their quantitative influence being given in Fig. 2.

Concerning the analysis of a batch reactor, which is the subject of section 3, Ha decreases with time due to the depletion of A, whereas C_{BS}^* increases from zero (at the beginning of electrolysis where $C_{BO} = 0$) to infinity. Therefore, considering Fig. 2, there is no simple way of predicting the type of change of i^* (increase or decrease) during the progression of the reaction.

3. Modelling of a batch stirred-tank electrochemical reactor (dynamic analysis)

3.1. *Case of the simplified chemical mechanism, scheme II [1]*

The modelling of a batch reactor can easily be performed on the basis of the study of a continuous stirred-tank reactor (CSTR), extending it to a piston flow reactor, PFR (approximating a PFR as a cascade of a large number, n, of CSTRs in series) and then to a batch reactor, since the space time, τ, of the PFR is simply replaced by the time, t. This classic procedure in chemical reaction engineering [6] is illustrated in Fig. 4.

In the case of the ith CSTR, operating under steady, continuous flow conditions, the inlet and outlet concentrations of A and B are respectively denoted ($C_{AS,i-1}$; $C_{BS,i-1}$) and ($C_{AS,i}$; $C_{BS,i}$).

The calculation method of a CSTR is based on writing the mass balances of species A and B in each of the two zones defining the reactor, i.e. the bulk and the film near the working electrode. This leads to the following relations.

(i) In the bulk:

$$Q_V C_{AS,i-1} = Q_V C_{AS,i} + k_c C_{AS,i} C_{BS,i} V + D_A A_e \left(\frac{dC_A}{dy}\right)_{y=\delta} \tag{12}$$

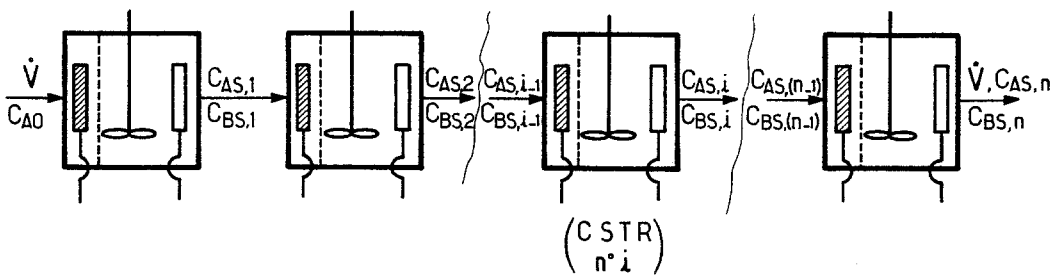

Fig. 4. Schematic diagram of a series of CSTRs as a model for a piston flow reactor.

and a similar expression for B. The last term corresponds to the flux of A at the limit of the two zones.

(ii) In the diffusion layer the mass balances are represented by Equations 1 and 2, which should be solved with the same boundary conditions as for Equations 1 and 2.

Using reduced variables leads to the following dimensionless quantities:

$$y^+ = y/\delta \tag{13$_1$}$$

$$C^+_{AO} = C_A/C_{AO} \text{ (inside the diffusion layer)} \tag{13$_2$}$$

$$C^+_{BO} = C_B/C_{AO} \tag{13$_3$}$$

$$C^+_{AS,i} = C_{AS,i}/C_{AO} \text{ (in the bulk)} \tag{13$_4$}$$

$$D^+_B = D_B/D_A \tag{13$_5$}$$

$$Ha^2_0 = \frac{k_c D_A C_{AO}}{k^2_d} \tag{13$_6$}$$

$$K_1 = k_c \tau C_{AO} \tag{13$_7$}$$

$$K_2 = k_d a_e \tau \tag{13$_8$}$$

where $\tau = V/Q_V$ is the space time of the electrolyte and $a_e = A_e/V$ is the specific electrode area.

It should be noted that, compared to the previous analysis of section 2 (which was a static analysis), C^+_{AO}, C^+_{BO} and Ha^2_0 here represent dimensionless quantities formally identical to those used in section 2 but based on the inlet concentration C_{AO} in the first reactor (see Fig. 4).

The following mass balance equations are then obtained:

(i) In the bulk

$$\begin{cases} C^+_{AS,i}(1 + K_1 C^+_{BS,i}) + K_2 \left(\dfrac{dC^+_{AO}}{dy^+}\right)_{y^+=1} = C^+_{AS,i-1} & (14_1) \\ C^+_{BS,i}(1 + K_1 C^+_{AS,i}) + K_2 D^+_B \left(\dfrac{dC^+_{BO}}{dy^+}\right)_{y^+=1} = C^+_{BS,i-1} & (14_2) \end{cases}$$

(ii) In the diffusion layer

$$\begin{cases} \dfrac{d^2 C^+_{AO}}{dy^{+2}} - Ha^2_0 C^+_{AO} C^+_{BO} = 0 & (15_1) \\ D^+_B \dfrac{d^2 C^+_{BO}}{dy^{+2}} - Ha^2_0 C^+_{AO} C^+_{BO} = 0 & (15_2) \end{cases}$$

with the boundary conditions

$$y^+ = 1; \quad C^+_{AO} = C^+_{AS,i}; \quad C^+_{BO} = C^+_{BS,i}$$

$$y^+ = 0 \begin{cases} C^+_{AO} = 0 \\ \left(\dfrac{dC^+_{AO}}{dy^+}\right) = -D^+_B \left(\dfrac{dC^+_{BO}}{dy^+}\right) \end{cases}$$

By considering Equations 13, 14 and 15, the performance of the reactor only depends on three dimensionless numbers: Ha^2_0, K_1 and K_2. The physical meaning of Ha^2_0 has already been discussed; K_1 and K_2 are operating criteria related to the geometry and mixing state of the cell. In the general case, the system of Equations 14 and 15 cannot be solved analytically and requires numerical integration.

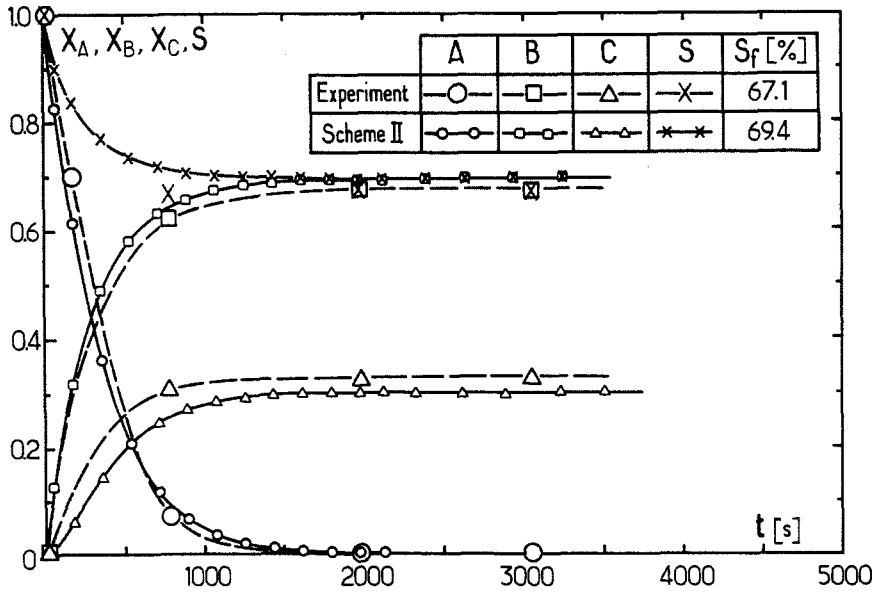

Fig. 5. Calculated time variations of the molar fractions X_A, X_B, X_C and selectivity S for reaction scheme II. Comparison with the experimental results. $C_{AO} = 62.87\,\text{mol}\,\text{m}^{-3}$; $T = 302\,\text{K}$; $N = 1000\,\text{r.p.m}$; $a_e = 115.3\,\text{m}^{-1}$.

In principle, a numerical method identical to the one presented in section 2 can be used here with the difference that the boundary conditions at $y^+ = 1$ must verify the mass balance equation (14_1 and 14_2) in the bulk of the CSTR. As mentioned previously, the calculation procedure for the batch reactor is obtained by repeating the calculation of a single CSTR (see Fig. 4) n times using a sufficiently small space time, $\Delta\tau$, of 30 s (equivalent to an increment of time Δt) for each reactor. It should be mentioned that the numerical integration is quite long: 250 mn CPU for simulating 80 mn of batch reactor time with a Honeywell Bull Mini 6/92 computer.

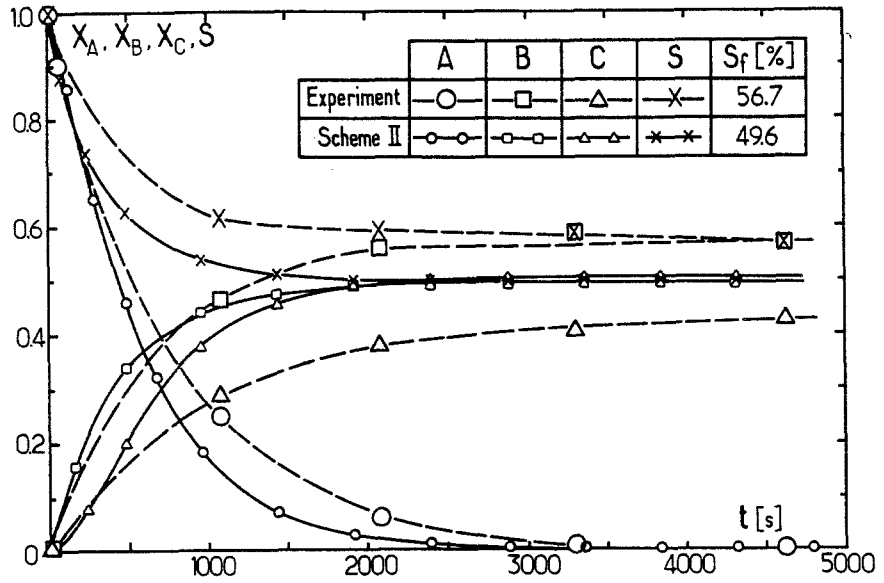

Fig. 6. Calculated time variations of the molar fractions X_A, X_B, X_C and selectivity S for reaction scheme II. Comparison with the experimental results. $C_{AO} = 103.24\,\text{mol}\,\text{m}^{-3}$; $T = 294\,\text{K}$; $N = 1000\,\text{r.p.m.}$; $a_e = 42.7\,\text{m}^{-1}$.

Figs 5 and 6 present some theoretical results calculated by this method for two different sets of operating conditions and compare them to the corresponding experimental time variations of the mole fractions X_A, X_B and X_C inside the cell. Examination of these figures shows that the agreement is very satisfactory, particularly for the conditions of Fig. 5. An important point concerns the calculated variation of the selectivity, S, which decreases continuously from 100% to a final value, S_f, obtained when $C_{AS} = 0$. The initial value of S (100%) is inherent to the type of simplified scheme II used in the mathematical model, but there is no experimental evidence to confirm this result due to the lack of experimental points at the very beginning of the experiments.

3.2. *Case of the complete chemical mechanism, scheme I [1]*

In Part I of this work [1] it has been shown that the simplified scheme II could give a good representation of the homogeneous chemical reaction between A and B, but that a more realistic reaction sequence involved the four mechanisms reported in Table 1. The chemical rate constants, k_{ci}, in this sequence were deduced approximately by a best-fit method using some experimental results presented in Part I (see Table 2 of Part I). Using a similar integration method as above for a batch reactor, we have calculated the time variations of the fractions X_A, X_B and X_C, starting the calculation of a single CSTR and extending it to the batch mode of operation (Fig. 4).

For the ith CSTR, the mass balance equations and the corresponding boundary conditions are summarized in Tables 2 and 3. The conservation equations were applied in both catholyte and the catholyte boundary layer and represent transport by diffusion with simultaneous homogeneous chemical reactions neglecting ionic migration. Compared to the case in section 3.1, the calculation time on a Mini 6/92 computer is even higher due to the more complex reaction sequence involved: 600 mn CPU for 15 min batch reaction time.

For the operating conditions considered in Figs 5 and 6, Figs 7 and 8 present the theoretical time variations of X_A, X_B, X_C and S using scheme I and compare them to the experimental results. As can be seen, the agreement is quite satisfactory for both types of experiments though the experimental values of the final selectivity, S_f, are always higher (about 7%) than those predicted by the model using scheme I. Furthermore, by comparing the calculated variations using schemes I and II (see, for example, Figs 6,8), it can be concluded that the simplified scheme II constitutes a very good approximation for all the chemical mechanisms involved. A small difference exists, however, if one considers the initial value of the selectivity which is 100% for scheme II and zero for scheme I: this observation may be explained by the chemical generation of species NO^+ (see first mechanism of Table 1) which occurs before the third mechanism at the beginning of an experiment.

In conclusion, for the *N*-amino-2-methylindoline system, it might be very useful to incorporate scheme II in an engineering model of an electrolytic cell since, in this case, the computation times as well as the data base needed (transport properties, chemical rate constants) are much smaller.

Table 1. Homogeneous chemical reactions and kinetic laws involved in scheme I

Homogeneous chemical reactions	*Kinetic laws*
$A + H^+ \underset{r_{-1}}{\overset{r_1}{\rightleftharpoons}} C + NO^+$	$r_1 = k'_{C1} C_A$; $k'_{C1} = k_{C1}[H^+]$ $r_{-1} = k_{C-1} C_C C_{NO^+}$
$NO^+ + EtOH \xrightarrow{r_2} EtONO + H^+$	$r_2 = k'_{C2} C_{NO^+}$; $k'_{C2} = k_{C2}[EtOH]$
$B + NO^+ \xrightarrow{r_3} C + N_2O + H^+$	$r_3 = k_{C3} C_B C_{NO^+}$
$B + H^+ \underset{r_{-4}}{\overset{r_4}{\rightleftharpoons}} BH^+$	$r_4 = k'_{C4} C_B$; $k'_{C4} = k_{C4}[H^+]$ $r_{-4} = k_{C-4} C_{BH^+}$

Table 2. Mass balance equations for the continuous stirred-tank electrochemical reactor with row 'i' (scheme I) when $y > \delta$

Species	*Mass balances ($y > \delta$)*
A	$Q_v C_{AS,i-1} = V(r_1 - r_{-1})_{y=\delta} + D_A A_e \left(\frac{dC_A}{dy}\right)_{y=\delta} + Q_v C_{AS,i}$
B	$Q_v C_{BS,i-1} = V(r_3 + r_4 + r_{-4})_{y=\delta} + D_B A_e \left(\frac{dC_B}{dy}\right)_{y=\delta} + Q_v C_{BS,i}$
BH^+	$Q_v C_{BH+S,i-1} = V(-r_4 + r_{-4})_{y=\delta} + D_{BH+} A_e \left(\frac{dC_{BH}}{dy}\right)_{y=\delta} + Q_v C_{BH+S,i}$
C	$Q_v C_{CS,i-1} = V(-r_1 + r_{-1} - r_3)_{y=\delta} + D_C A_e \left(\frac{dC_C}{dy}\right)_{y=\delta} + Q_v C_{CS,i}$
NO^+	$Q_v C_{NO+S,i-1} = V(-r_1 + r_{-1} + r_2 + r_3)_{y=\delta} + D_{NO+} A_e \left(\frac{dC_{NO+}}{dy}\right)_{y=\delta} + Q_v C_{NO+S,i}$

4. Approximate analytical model of batch electrolytic cell for small Hatta number (simplified chemical scheme)

The effect of the chemical rate constant, k_c, on the instantaneous current density was studied theoretically in section 2 for a potentiostatic operation. It has been shown that for a small Hatta number, the dimensionless form, i^*, of the current density remains close to 1 (see Fig. 2), i.e. that at any time: $i = i_L = v_e F k_d C_{AS}$.

In fact, this implies that the chemical reaction in the boundary layer at the working electrode may be neglected and consequently that the concentration profiles of A and B are linear at any time in the layer of thickness δ. With this approximation, the mathematical model is greatly simplified since the conservation equations of A and B in the bulk take the following forms:

Table 3. Mass balance equations for the continuous stirred-tank electrochemical reactor with row 'i' (scheme I) when $0 < y < \delta$

Species	*Mass balances for $0 < y < \delta$*	*Boundary conditions*	
		When $y = 0$	*When $y = \delta$*
A	$D_A \left(\frac{d^2 C_A}{dy^2}\right) = r_1 - r_2$	$D_A \left(\frac{dC_A}{dy}\right)_{y=0} = \frac{i}{v_e F}$; $(C_A)_{y=0} = 0$	$(C_A)_{y=\delta} = C_{AS,i}$
B	$D_B \left(\frac{d^2 C_B}{dy^2}\right) = r_3 + r_4 - r_{-4}$	$D_B \left(\frac{dC_B}{dy}\right)_{y=0} = 0$	$(C_B)_{y=\delta} = C_{BS,i}$
BH^+	$D_{BH+} \left(\frac{d^2 C_{BH+}}{dy^2}\right) = -r_4 + r_{-4}$	$D_{BH+} \left(\frac{dC_{BH+}}{dy}\right)_{y=0} = -\frac{i}{v_e F}$	$(C_{BH+})_{y=\delta} = C_{BH+S,i}$
C	$D_C \left(\frac{d^2 C_C}{dy^2}\right) = -r_1 + r_{-1} - r_3$	$D_C \left(\frac{dC_C}{dy}\right)_{y=0} = 0$	$(C_C)_{y=\delta} = C_{CS,i}$
NO^+	$D_{NO+} \left(\frac{d^2 C_{NO+}}{dy^2}\right) = -r_1 + r_{-1} + r_2 + r_3$	$D_{NO+} \left(\frac{dC_{NO+}}{dy}\right)_{y=0} = 0$	$(C_{NO+})_{y=\delta} = C_{NO+S,i}$

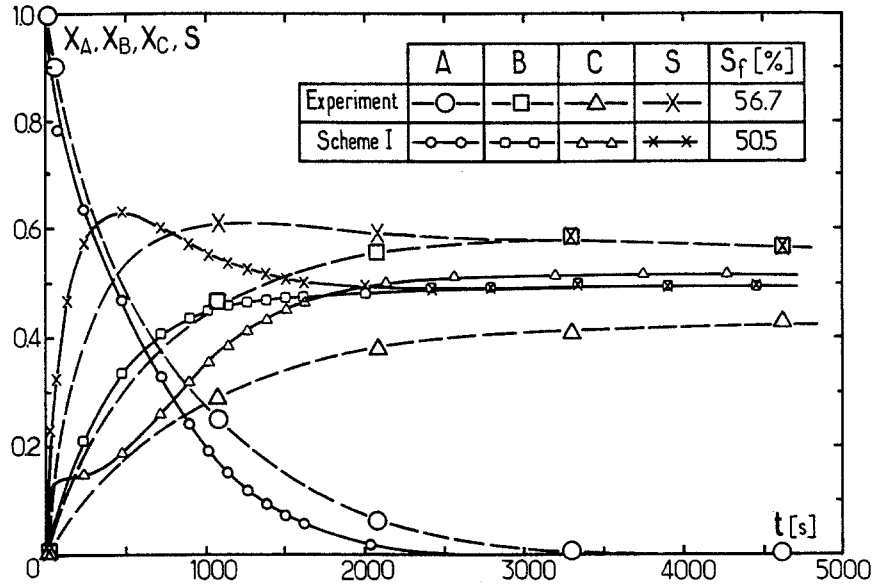

Fig. 7. Calculated time variations of the molar fractions X_A, X_B, X_C and selectivity, S, for reaction scheme I (operating conditions of Fig. 5). Comparison with the experimental results. $C_{AO} = 62.87\,\text{mol}\,\text{m}^{-3}$; $T = 302\,\text{K}$; $N = 1000\,\text{r.p.m}$; $a_e = 115.3\,\text{m}^{-1}$.

$$\begin{cases} V\dfrac{dC_{AS}}{dt} + k_c C_{AS} C_{BS} V + k_d A_e C_{AS} = 0 & (16_1) \\ V\dfrac{dC_{BS}}{dt} + k_c C_{AS} C_{BS} V - k_d A_e C_{AS} = 0 & (16_2) \end{cases}$$

The last terms of Equations 16_1 and 16_2 correspond to the flux of A and B at the limit of the

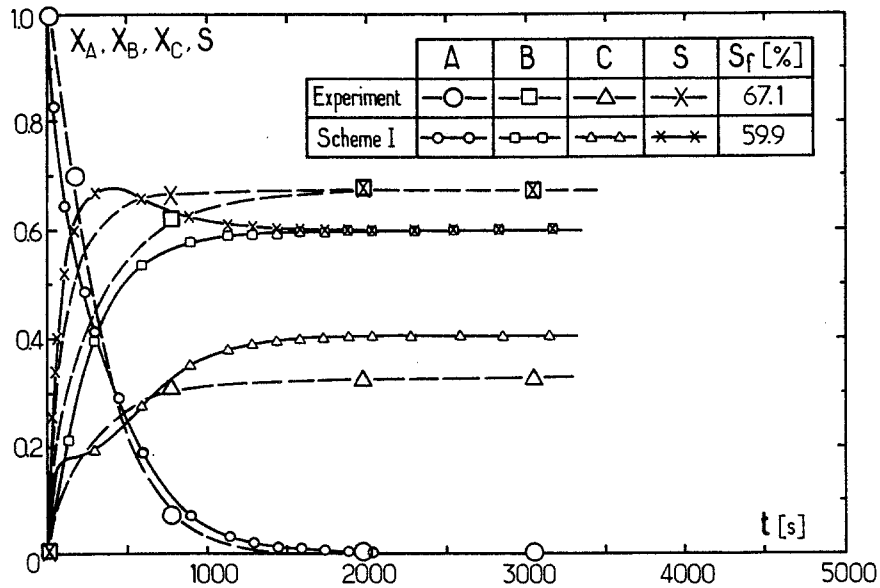

Fig. 8. Calculated time variations of the molar fractions X_A, X_B, X_C and selectivity, S, for reaction scheme I (operating conditions of Fig. 6). Comparison with the experimental results. $C_{AO} = 103.24\,\text{mol}\,\text{m}^{-3}$; $T = 294\,\text{K}$; $N = 1000\,\text{r.p.m}$; $a_e = 42.7\,\text{m}^{-1}$.

boundary layer, which now have a simplified expression due to the linear variations of C_A and C_B in the boundary layer.

Under dimensionless form, Equations 16_1 and 16_2 are reduced to

$$\begin{cases} \dfrac{dC_{AS}^+}{dt^+} + KC_{AS}^+ C_{BS}^+ + C_{AS}^+ = 0 & (17_1) \\ \dfrac{dC_{BS}^+}{dt^+} + KC_{AS}^+ C_{BS}^+ - C_{AS}^+ = 0 & (17_2) \end{cases}$$

with

$$C_{AS}^+ = C_{AS}/C_{AO},\ C_{BS}^+ = C_{BS}/C_{AO}$$
$$t^+ = t(k_d a_e)$$

and

$$K = \frac{k_c C_{AO}}{k_d a_e} = \frac{K_1}{K_2} = \frac{k_c C_{AO}^2 V}{k_d A_e C_{AO}}$$

The boundary conditions for $t^+ = 0$ are: $C_{AS}^+ = 1$; $C_{BS}^+ = 0$

In Equations 17_1 and 17_2, t^+ is a dimensionless form of the electrolysis time, t, whereas K is a criterion governing the overall process selectivity. Compared to the Ha_0^2 number introduced in section 3.1, which gives a quantitative evaluation of the competition between the chemical and electrochemical reaction rates in the diffusion boundary layer, K has a similar meaning concerning the competition occurring in the bulk.

No analytical solution of Equation 17 exists, but the variations of S with the conversion factor of the reactant A are easily found analytically. Indeed, dividing Equation 17_1 by 17_2 gives simply:

$$\frac{dC_{AS}^+}{dC_{BS}^+} = \frac{KC_{BS}^+ + 1}{KC_{BS}^+ - 1} \qquad (18)$$

which after integration leads to the relation between C_{AS}^+ and C_{BS}^+:

$$C_{AS}^+ - 1 = C_{BS}^+ + 2/K \ln (1 - KC_{BS}^+) \qquad (19)$$

Equation 19 relates the conversion factor $R_A = 1 - C_{AS}^+$ of the reactant A to the product KC_{BS}^+:

$$KR_A + KC_{BS}^+ + 2 \ln (1 - KC_{BS}^+) = 0 \qquad (20)$$

Furthermore, the instantaneous selectivity, S, may be expressed as

$$S = \frac{C_{BS}}{C_{AO} - C_{AS}} = \frac{C_{BS}^+}{1 - C_{AS}^+} = \frac{KC_{BS}^+}{KR_A}$$

Elimination of KC_{BS}^+ between Equations 20 and 21 yields the curve shown in Fig. 9 which gives the theoretical variation of S with $K(1 - C_{AS}^+)$.

It should be mentioned that during an experiment, S varies from 1 (at $t = 0$) to a final value S_f (for $t \to \infty$) which corresponds in Fig. 9 to the ordinate obtained for the value K of the abcissa (since $C_{AS}^+ \to 0$ for $t \to \infty$). The validity of this mathematical development, leading to an analytical expression of the selectivity, has been verified by showing experimental results of S_f (Fig. 9), obtained under very different operating conditions presented in Table 4. As can be seen, the experimental points are found to be in very good agreement with the theoretical curve. It should be remembered that this mathematical model is restricted to the case where i^* remains close to 1 during the extent of the reaction, i.e. for sufficiently small values of the Hatta number. By considering the conditions of Table 4, it can be shown that this hypothesis is effectively valid since Ha_0 is smaller than

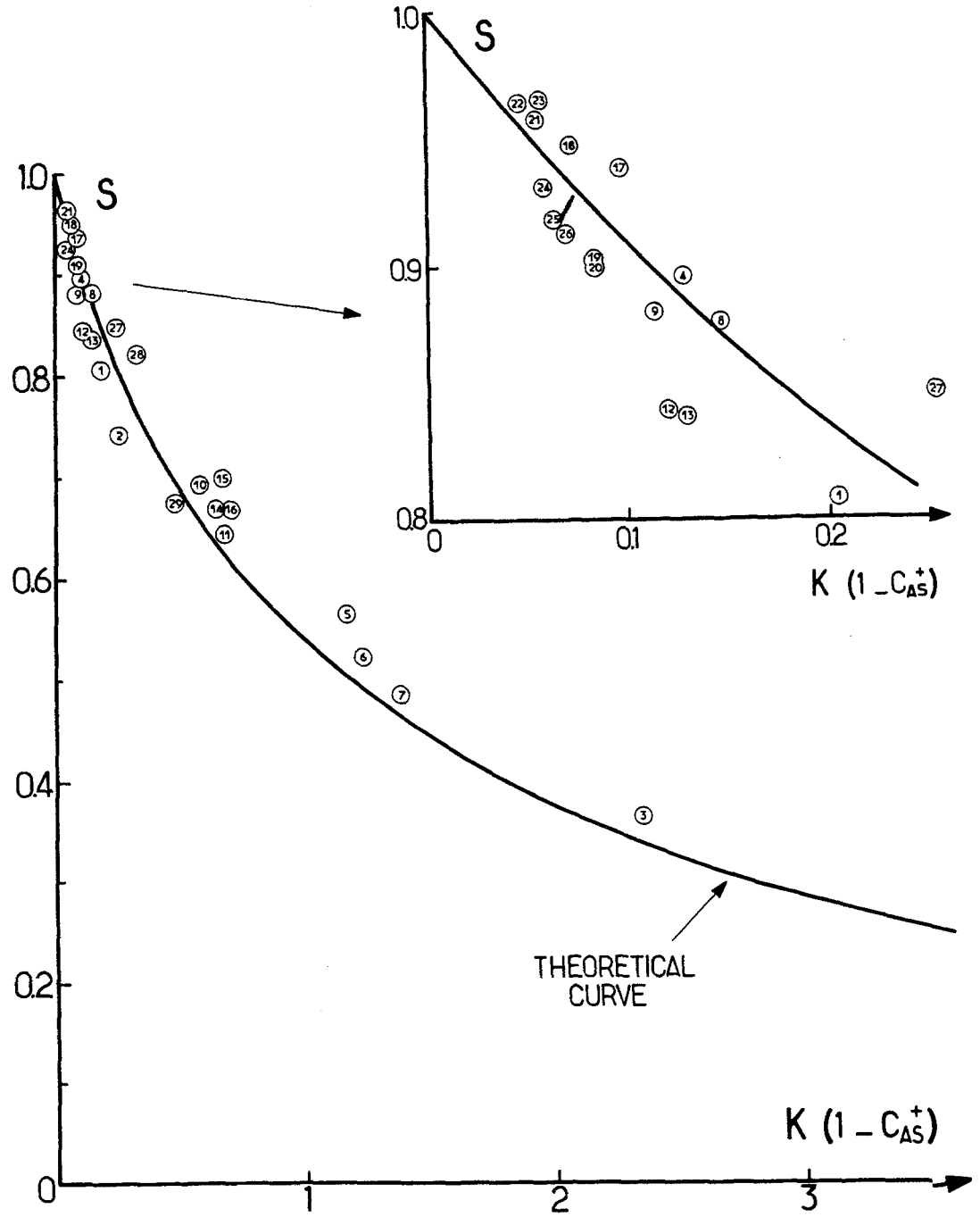

Fig. 9. Theoretical variations of the selectivity, S, with the product $K(1 - C_{AS}^{+})$. Comparison with the experimental results (the numbers correspond to the operating conditions of Table 4).

3.7×10^{-2} for all experiments considered. In Fig. 9 the comparison was restricted to the final selectivity, S_f, but the good agreement between model and experiment was also verified for the instantaneous selectivity.

Consequently, this analytical engineering model of a batch stirred-tank electrochemical reactor

Table 4. Values of the final selectivity, S_f, obtained under different experimental conditions

No.	a_e *(m^{-1})*	T *(K)*	N *(r.p.m.)*	C_{AO} *($mol\,m^{-3}$)*	E *versus SCE (V)*	K	Ha_o	k_d *($m\,s^{-1}$)*	S_f *(%)*
1	42.7	298.0	500	9.04	−0.8	0.206	1.119×10^{-2}	1.75×10^{-5}	80.9
2	42.7	298.0	500	11.77	−0.8	0.267	1.259×10^{-2}	1.75×10^{-5}	73.9
3	42.7	298.0	500	102.90	−0.9	2.342	3.271×10^{-2}	1.75×10^{-5}	36.7
4	42.7	298.0	1000	9.98	−0.8	0.128	6.586×10^{-3}	3.11×10^{-5}	89.5
5	42.7	294.1	1000	103.24	−0.85/−1.5	1.177	1.635×10^{-2}	3.11×10^{-5}	56.7
6	42.7	294.1	1000	96.31	−0.85/−1.5	1.234	1.782×10^{-2}	3.11×10^{-5}	51.8
7	42.7	294.1	1000	106.95	−0.75/−0.9	1.370	1.876×10^{-2}	3.11×10^{-5}	48.4
8	115.3	283.4	250	10.45	−1.0	0.147	1.694×10^{-2}	6.722×10^{-6}	87.8
9	115.3	295.0	250	8.92	−0.9	0.113	1.612×10^{-2}	1.07×10^{-5}	88.2
10	115.3	291.0	250	50.70	−0.83	0.569	3.035×10^{-2}	1.07×10^{-5}	69.5
11	115.3	293.7	250	55.89	−0.9	0.680	3.475×10^{-2}	1.07×10^{-5}	64.4
12	115.3	296.3	250	9.10	−0.9	0.119	1.714×10^{-2}	1.07×10^{-5}	84.3
13	115.3	297.0	250	9.55	−0.9	0.128	1.802×10^{-2}	1.07×10^{-5}	84.1
14	115.3	295.8	250	50.08	−1.0/−1.6	0.648	3.534×10^{-2}	1.07×10^{-5}	67.2
15	115.3	297.0	250	49.95	−1.0/−1.6	0.669	3.682×10^{-2}	1.07×10^{-5}	69.7
16	115.3	297.0	250	50.61	−1.0/−1.6	0.678	3.704×10^{-2}	1.07×10^{-5}	67.2
17	115.3	283.2	500	10.53	−1.0	9.945×10^{-2}	1.136×10^{-2}	9.970×10^{-6}	93.8
18	131.8	296.0	500	9.51	−0.9	7.193×10^{-2}	1.148×10^{-2}	1.61×10^{-5}	94.7
19	115.3	297.1	500	9.82	−0.9	8.767×10^{-2}	1.217×10^{-2}	1.61×10^{-5}	90.2
20	115.3	297.6	500	9.82	−0.9	8.895×10^{-2}	1.242×10^{-2}	1.61×10^{-5}	90.2
21	115.3	287.8	1000	10.45	−1.0	5.488×10^{-2}	6.262×10^{-3}	1.77×10^{-5}	95.8
22	115.3	295.5	1000	8.00	−0.9	4.921×10^{-2}	7.520×10^{-3}	2.23×10^{-5}	96.4
23	115.3	295.9	1000	9.10	−0.9	5.664×10^{-2}	8.093×10^{-3}	2.23×10^{-5}	96.5
24	115.3	296.4	1000	9.28	−0.9	5.861×10^{-2}	8.330×10^{-3}	2.23×10^{-5}	93.3
25	115.3	297.7	1000	9.60	−0.9	6.296×10^{-2}	8.915×10^{-3}	2.23×10^{-5}	91.7
26	115.3	297.1	1000	10.49	−0.9	6.736×10^{-2}	9.033×10^{-3}	2.23×10^{-5}	91.4
27	115.3	296.0	1000	40.55	−1.0/−1.6	0.253	1.551×10^{-2}	2.23×10^{-5}	84.9
28	115.3	298.0	1000	50.00	−1.0/−1.6	0.331	1.835×10^{-2}	2.23×10^{-5}	82.1
29	115.3	302.0	1000	62.87	−0.8	0.466	2.475×10^{-2}	2.23×10^{-5}	67.1

is perfectly adapted to the prediction of the selectivity in the *N*-amino-2-methylindoline electrochemical process.

5. Conclusions

This work has presented an engineering model of a batch or a continuous stirred-tank electrochemical reactor where simultaneous homogeneous chemical and electrochemical heterogeneous reactions occur. The example of *N*-amino-2-methylindoline synthesis has been used for illustrating the procedure followed in this study, since comparison of the theoretical results to those deduced from an experimental approach demonstrates the validity of the mathematical simulation and quantifies its accuracy. As the level of sophistication of the chemical reaction sequence coupled with the electrochemical desired reaction increases, it may be interesting as a first approximation to consider a simplified chemical scheme in the model when the data base (transport properties, rate constants) is insufficient, necessitating further difficult experiments, and the computing time becomes too important. This is particularly true when economic optimization of the process has to be performed.

The possibility of deriving simple dimensionless quantities characterizing the cell performance and selectivity is an additional advantage of a simplified but realistic reaction scheme. For the *N*-amino-2-methylindoline system, the results obtained experimentally in a batch reactor are in excellent agreement with the predictions of the model which, therefore, can be extended in principle to other specific processes.

References

[1] L. Weise, G. Valentin and A. Storck, *J. Appl. Electrochem.* **16** (1986) 836.
[2] R. C. Alkire and J. D. Lisius, *J. Electrochem. Soc.* **132** (1985) 1879.
[3] P. V. Danckwerts, 'Gas–Liquid Reactions', Mc-Graw Hill, New York (1970).
[4] J. C. Charpentier and G. Wild, 'Absorption avec réaction chimique', Technique de l'Ingénieur, J2640-12, Paris (1983).
[5] W. H. Ray and J. Szekely, 'Process Optimization', John Wiley and Sons, New York (1983).
[6] J. Villermaux, 'Génie de la Réaction Chimique', Technique et Documentation, Lavoisier, Paris (1982).